Highlights

Compact Polarization-Reconfigurable AFSIW Array with Integrated Biasing Network

- First air-filled substrate integrated waveguide (AFSIW) scalable polarization-reconfigurable antenna array with switchable $\pm 45^{\circ}$ linear polarization states
- An integrated biasing network eliminating any discrete components and enabling low power consumption
- High radiation efficiency within a compact footprint ($0.6\lambda_0 \times 0.6\lambda_0$), enabling beam steering

Compact Polarization-Reconfigurable AFSIW Array with Integrated Biasing Network

Victor Van der Elst[a], Kamil Yavuz Kapusuz[a], Sam Lemey[a], Jo Verhaevert[a], Hendrik Rogier[a]

[a]*Department of Information Technology, IDLab/EM Group, Ghent University/IMEC, Technologiepark-Zwijnaarde 126, Ghent, 9052, Belgium*

Abstract

A polarization-reconfigurable antenna array with an integrated biasing network is demonstrated using air-filled substrate-integrated waveguide (AFSIW) technology for the [7.75–8.25] GHz sub-band of Frequency Range 3 (FR3). The antenna element features a compact $0.6\lambda_0 \times 0.6\lambda_0$ footprint, utilizing a U-shaped slot within a quarter-mode AFSIW topology. Two PIN diodes enable +45°/-45° polarization switching by electrically shorting the slot at well-defined positions. Their DC bias is provided through inductive vias, which are isolated by capacitive gaps, allowing seamless integration without additional biasing components. The stand-alone antenna prototype was fabricated using low-cost printed circuit board (PCB) technology. Moreover, a 2×2 array was fabricated to validate the platform's scalability. Measurements reveal a -10 dB impedance bandwidth of 590 MHz (7.46%) for both the single element and the array. The stand-alone antenna achieves a peak gain of 5.18 dBi, 91% efficiency, and 16.5 dB boresight cross-polarization discrimination across the entire frequency band. The array achieves a peak realized gain of 9.5 dBi, with embedded element radiation patterns closely matching the single-element patterns owing to mutual coupling remaining below -15 dB. 2D steering was demonstrated in simulation for a 4×4 array up to 40°. Measurement results align closely with simulations, confirming effective polarization reconfigurability, making the design well-suited for next-generation FR3 communication systems.

Keywords: Polarization-reconfigurable antennas, air-filled substrate integrated waveguide (AFSIW) technology, integrated biasing network, beam steering

---

1. Introduction

Wireless communication has revolutionized how information is transmitted and received, enabling seamless connectivity for countless applications ranging from mobile telephony to the Internet of Things (IoT) [1]. Antennas play an essential role in these systems, serving as the critical interface between radio frequency (RF) signals and the physical environment. Antenna design profoundly impacts system performance, influencing factors such as signal coverage, link reliability, and spectral efficiency [2]. As wireless networks evolve, the demand for antennas that are compact, energy-efficient, and capable of adaptive operation continues to grow [3].

Sixth-generation (6G) networks are poised to further transform wireless communication systems by providing ultra-high data rates and ultra-low latency. Especially, the [7.125-24.25] GHz FR3 band emerges as a crucial resource, offering superior bandwidth compared to the sub-7 GHz FR1 band, along with more favorable propagation characteristics than the [24.25-71] GHz FR2 band, making the FR3 band better suited to meet the demands of future network applications [4]. Notably, the [7.125–24.25] GHz FR3 band encompasses the IEEE 802.15.4z UWB Channel 9 band (7.737–8.236 GHz), opening opportunities for future research in UWB-based high-precision positioning applications such as indoor localization and asset tracking, but also for future 6G use cases. The integration of polarization reconfigurability further enables rotation and orientation estimation, enhancing the accuracy of such systems.

However, this FR3 band is still susceptible to path loss, which can be overcome by employing highly directive antenna arrays (AAs). Secondly, the ecological challenge in this 6G revolution requires energy-efficient designs [1]. While beamforming vastly improves signal range and enables spatial filtering, polarization-reconfigurable antennas can adapt to changing conditions, mitigating multipath fading, and optimizing efficiency, while keeping hardware cost and complexity low in comparison with multiple single-polarization antenna systems [2]. Such low-cost, power-efficient adaptability is crucial for improving wireless link reliability and maximizing spectral efficiency in 6G networks, where compact, agile, and highly efficient antenna solutions are increasingly required.

Cavity-backed antennas implemented using substrate integrated waveguide (SIW) or air-filled substrate integrated waveguide (AFSIW) technology have emerged as promising candidates for 6G communication systems, thanks to their cost-effective fabrication [5, 6] and inherent self-shielding characteristics [7, 8]. Additionally, SIW structures enable compact integrated circuit (IC) integration, facilitating compact fully-integrated front-ends for applications such as radar and wireless sensing [9]. Furthermore, by employing air as the propagation medium in AFSIW-based systems, high efficiency and wideband performance can be achieved [10, 11]. AFSIW topologies have also been shown to be very robust with respect to temperature variations, as shown in [12]. For temperatures ranging from -40 °C to 80 °C, an AFSIW filter structure exhibits only a 24.9 MHz frequency shift at -40 °C and a -21.1 MHz drift at 80 °C. A drawback of AFSIW antennas, however, is their relatively large footprint, which makes them unsuitable for dense phased-array implementations; the limited number of elements within a given aperture reduces the achievable beam steering range [13]. To mitigate footprint constraints in AFSIW while enabling beam steering, capacitively loaded aperture-coupled stacked-patch configurations [14, 15] and quarter-mode SIW (QM-SIW) or quarter-mode AFSIW (QM-AFSIW) miniaturization techniques [16, 17] have been proposed. However, these only support a fixed single polarization, which limits their the ability to exploit diverse polarizations, which is essential in dynamic propagation environments.

Over the past decade, dynamic polarization reconfiguration in single-feed antennas has been actively investigated to to improve the reliability of wireless communication. Traditional methods, such as feed-line switching, can be used to activate specific modes within a cavity [18, 19], select certain feeding probes that enable different polarizations [20, 21, 22] or configure phase-delay lines to reconfigure the polarization [23]. These methods often increase system complexity and physical size, and they can cause electromagnetic interference (EMI) due to signal leakage [24, 25]. However, while reconfigurable radiator designs employing liquid metal [26, 27, 28], radiating slot reconfiguration [29], radiating patch reconfiguration [30, 31, 32, 33] or switchable probe designs [34, 35] have been proposed to address these challenges, they often require multiple discrete components and complex DC biasing systems. These solutions often lead to low radiation efficiency [29] and/or a large footprint [36, 31], which hinders their integration into antenna arrays and limits beam steering range. The large number of required components leads to significant power consumption, limiting the effectiveness of current systems for next-generation beamforming applications [20]. These challenges highlight the need for a polarization-reconfigurable antenna element that combines high radiation efficiency with a compact, array-compatible form factor.

This paper presents a novel polarization-reconfigurable antenna array tailored for compact, broadband, and efficient beam-steering applications, realized using a QM-AFSIW cavity-backed slot antenna operating in the [7.75–8.25] GHz FR3 band. The key innovation lies in the polarization reconfigurability, achieved by combining two L-shaped slots supporting $\pm 45°$ linear polarization (LP) into a single U-shaped radiating slot, enabling multiple polarization states within a compact, array-compatible footprint, which is particularly difficult to realize in air-filled designs [37]. The polarization state is dynamically selected via diode-controlled metal shorting tabs, implemented with an integrated bias-tee topology that leverages low-cost PCB fabrication techniques. Compared to conventional designs, like those requiring additional discrete components such as inductors for biasing [34, 35], the proposed integrated biasing network offers several advantages: it requires only two PIN diodes to switch between the $\pm 45°$ linear polarization states, eliminates the need for additional bias components, reduces PCB complexity, and minimizes insertion losses. The design achieves high radiation efficiency (>90%), while maintaining a compact footprint of $0.6\lambda_0 \times 0.6\lambda_0$. To achieve this, several challenges were addressed in the design process. Achieving compactness, while maintaining high efficiency necessitated careful slot shaping and precise placement of the shorting tabs. Additionally, integrating the biasing network into the antenna without compromising radiation performance required meticulous layout optimization. Potential disadvantages include the limited number of polarization states (restricted to two $\pm 45°$ states in the current design). To the best of the authors' knowledge, this is the first polarization-reconfigurable QM-AFSIW topology with an integrated biasing network operating in the FR3 band.

The structure of this paper is as follows. Section 2 outlines the antenna design process, details the proposed reconfigurable topology, explains its operating principles, and summarizes the final specifications. Section 3 then presents the simulation and measurement results and compares these to state-of-the art solutions. Lastly, the conclusions are drawn in section 4.

Funding

Part of this work was funded by the FWO research project 3G0B9821 "Safe HousePower".

2. Compact polarization-reconfigurable Antenna

2.1. Stand-alone antenna element (AE)

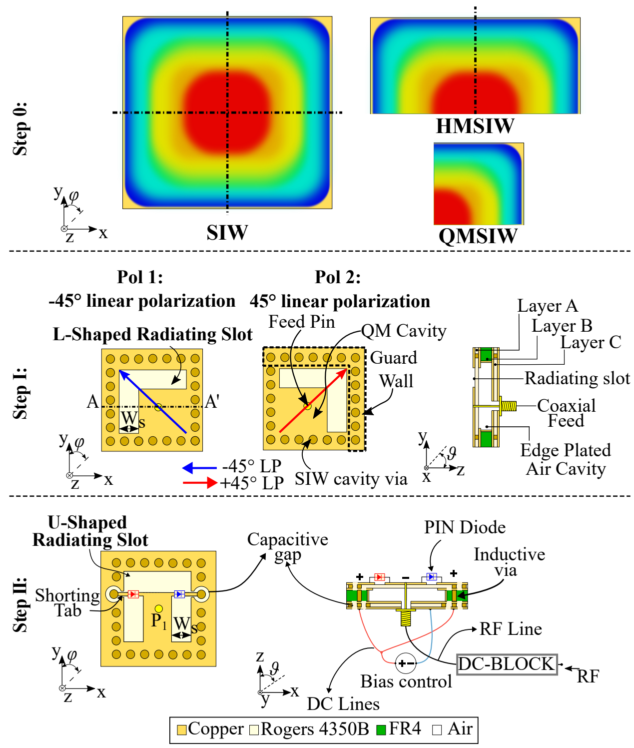

Figure 1: Two-step design process of the polarization-reconfigurable antenna element (AE) starting from a QM-AFSIW cavity. Step 0: From AFSIW to QM-AFSIW resonator. Step I: Design of two linearly polarized antennas using L-shaped slots to achieve orthogonal polarizations. Step II: Combines both L-shaped slots into a single U-shaped slot with embedded PIN diodes. Optimizing the placement of the diodes to enable polarization reconfiguration based on their switching states. The capacitive gap and inductive via form an integrated bias-tee. RF signals are routed through a DC block to protect the measurement equipment, while DC connections are made directly to the integrated bias-tee.

The proposed stand-alone antenna is shown in Fig. 1. It is implemented based on a two-step design process to achieve polarization reconfigurability within a compact, array-compatible form factor. First, an AFSIW cavity is calculated using Eq. (1) [37]. This cavity is then transformed into a QM-AFSIW cavity, as shown in Step 0 of Fig. 1.

$$f_{TE_{101}} = \frac{c}{2\pi\sqrt{\mu_r\varepsilon_r}}\sqrt{\left(\frac{\pi}{a_{\text{eff}}}\right)^2 + \left(\frac{\pi}{b_{\text{eff}}}\right)^2}, \tag{1}$$

The three-layer build-up as shown in Step I Fig. 1 is conceived as follows: a top plane (layer A) implementing the aperture, a middle dielectric plane (layer B) as the air-filled cavity with edge-plated sidewalls, and the bottom plane (layer C) as the cavity backplane. The air cavity realized by layer B allows for a highly efficient structure, owing to its low dielectric loss. A transverse electric magnetic (TEM) mode, introduced through a coaxial feed, excites a quarter transverse electric 110 (TE_{110}) mode within the cavity. A guard wall is introduced to isolate the elements in array configurations. The spacing W_s is then optimized to maximize radiation efficiency, while minimizing the antenna footprint (W_s = 5.3 mm), thereby enabling beam-steering. The polarization state is controlled through L-shaped radiating slots, supporting -45° LP (blue arrow) and +45° LP (red arrow), based on the slot orientation shown in Step I of Fig. 1.

Step II introduces polarization reconfigurability by merging and optimizing the two polarization states into one single element with a U-shaped radiating slot. Shorting tabs are initially introduced to segment the U-shaped slot into two L-shaped slots, with their placement dictating the LP direction based on the slot orientation given in Step I. Dynamic reconfiguration is realized by replacing these shorting tabs with PIN diodes. Simulations demonstrate that polarization purity remains above 15 dB when exploiting the PIN diodes for reconfiguration. The PIN diode positions are chosen as close as possible to the edge defining the same L-shaped slot as in step I, to avoid adding extra electrical length along that path, which would shift the frequency band of operation. PIN diodes of type MA4AGBLP912 [38] by MACOM are chosen because of their low resistance in their forward-biased state and low capacitance in their reverse-biased state. Their equivalent circuit in both states is depicted in Fig. 3, following the extracted values obtained in [36]. Applying only two PIN diodes per antenna element guarantees high radiation efficiency, owing to minimal extra resistance, low power consumption, and cost. Subsequently, controlling the two PIN diode states (red and blue in Step II) facilitates seamless switching between -45° LP, by forward-biasing the blue PIN diode while keeping the red PIN diode OFF, and applying the opposite bias to achieve the +45° LP, thereby enabling near-instant polarization switching.

The complete design procedure is summarized in a flowchart in Fig. 2.

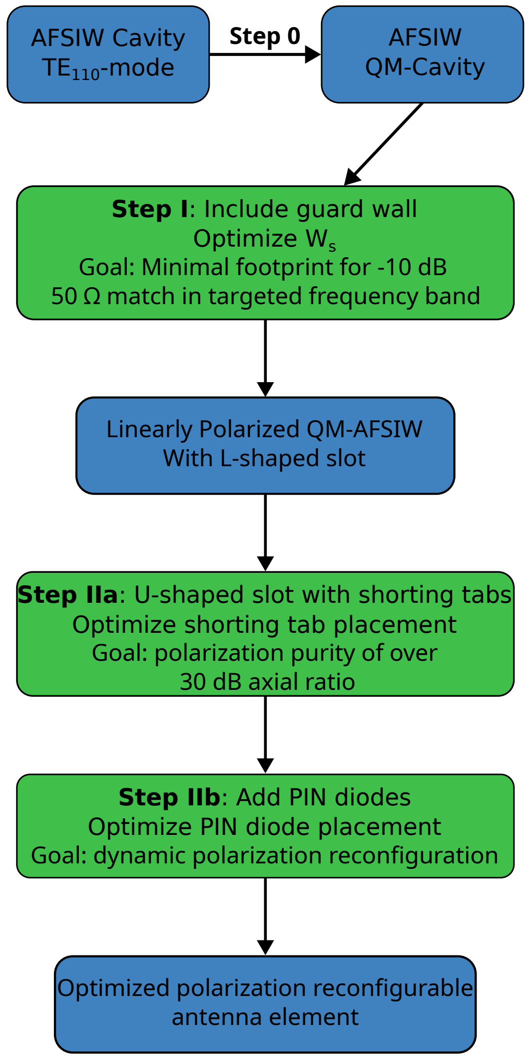

Figure 2: Flowchart summarizing the design procedure of the reconfigurable antenna.

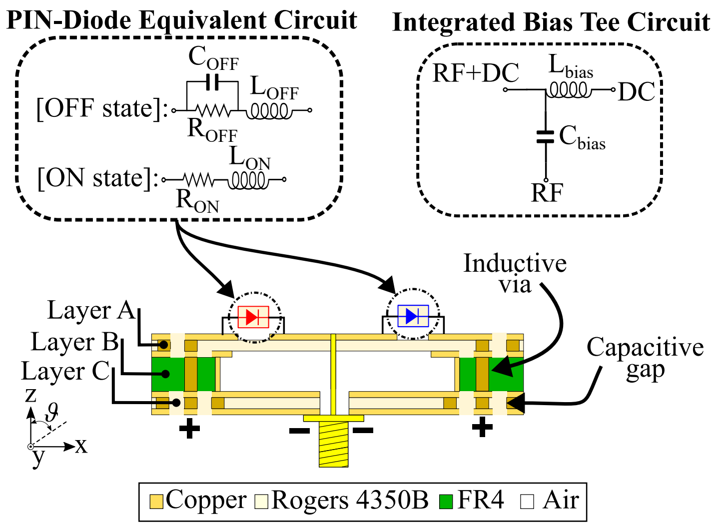

Figure 3: Integrated bias-tee and PIN-diode equivalent circuits. Values of the PIN diode are as follows: $C_{OFF} = 5$ fF, $R_{OFF} = 10$ kΩ, $L_{OFF} = 5.1$ nH, $R_{ON} = 5.5$ Ω, and $L_{ON} = 0.08$ nH. The bias-tee values are as follows: $L_{BIAS} = 0.95$ nH and $C_{BIAS} = 3.89$ pF [36].

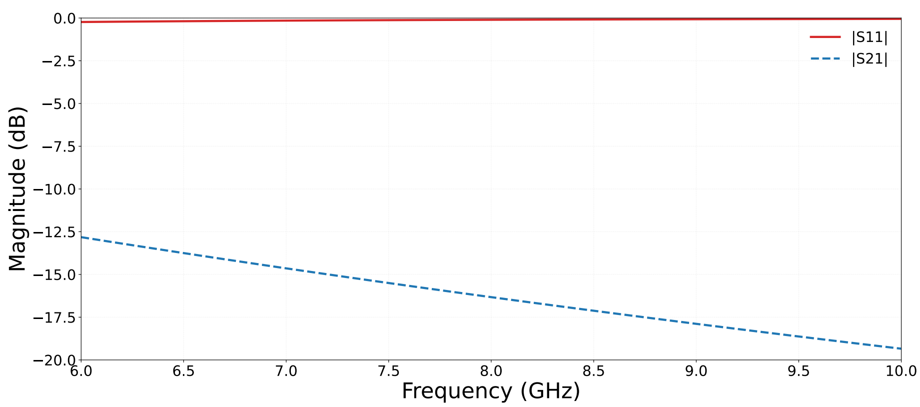

Figure 4: Bias-Tee isolation between RF+DC-line and DC-connection showing isolation of over 15dB for the targeted frequency band.

To enable dynamic and independent control of each PIN diode, capacitive gaps are introduced in both layer A and layer C of Fig. 3. These gaps effectively isolate the diodes at DC. The DC connection on layer A is then routed through plated inductive vias extending to the bottom of layer C. These vias function as RF chokes, enabling the DC bias current to flow from layer A to layer C of the antenna. The capacitive gaps and inductive vias together form an integrated bias-tee for the diodes, as illustrated in Fig. 3. The integrated bias-tee was simulated to show good isolation between its RF+DC-line and the DC-connection. Fig. 4 shows good isolation of over 15dB for the targeted frequency band, indicating that the RF signals are effectively blocked from propagating into the DC lines. This ensures that the DC biasing does not interfere with the RF performance, maintaining signal integrity and overall system stability. The vias used to construct the integrated bias-tee serve a dual purpose, also functioning as part of the guard walls introduced in Step I. Consequently, they also influence the overall size of the antenna. The antenna dimensions, optimized in CST Microwave Studio's electromagnetic field solver to cover the [7.75–8.25] GHz FR3 frequency band, are shown in Fig. 10, which also depicts the fabricated prototype. The 3D realized gain antenna radiation pattern is shown in Fig. 5 and 3D axial ratio pattern, indicating good linear polarization performance in both states, is shown in Fig. 6.

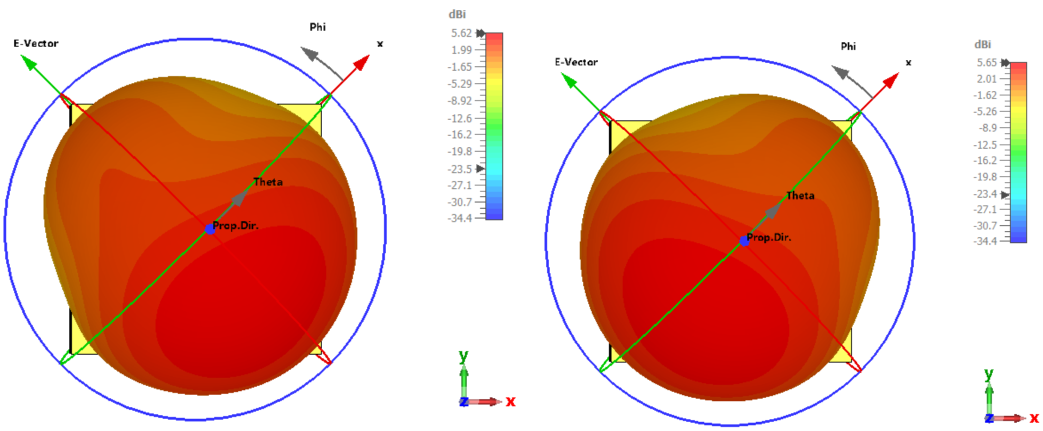

(a) (b)

Figure 5: 3D realized gain radiation patterns of proposed polarization-reconfigurable AF-SIW antenna element: (a) Pol. 1 (+45° linear polarization) state and (b) Pol. 2 (-45° linear polarization) state.

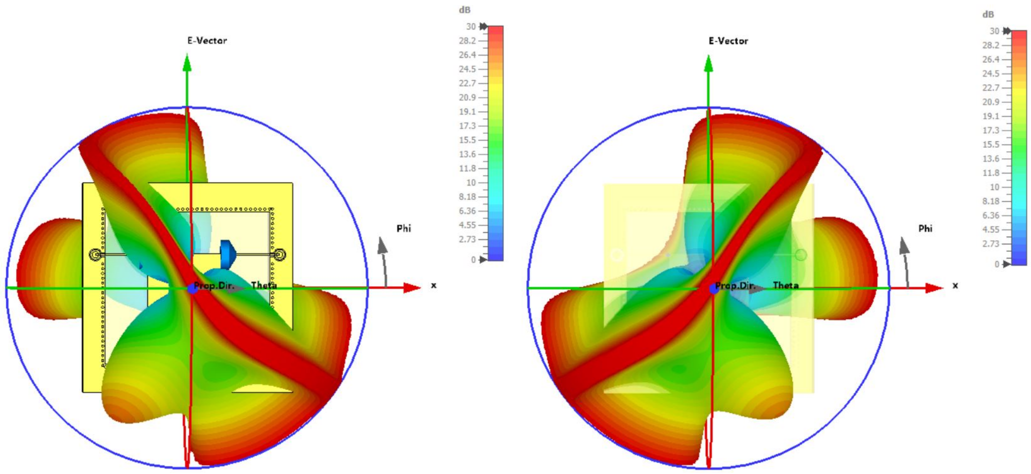

(a) (b)

Figure 6: Simulated 3D axial ratio patterns of proposed polarization-reconfigurable AF-SIW antenna element: (a) Pol. 1 (+45° linear polarization) state and (b) Pol. 2 (-45° linear polarization) state.

2.2. Antenna Array (AA)

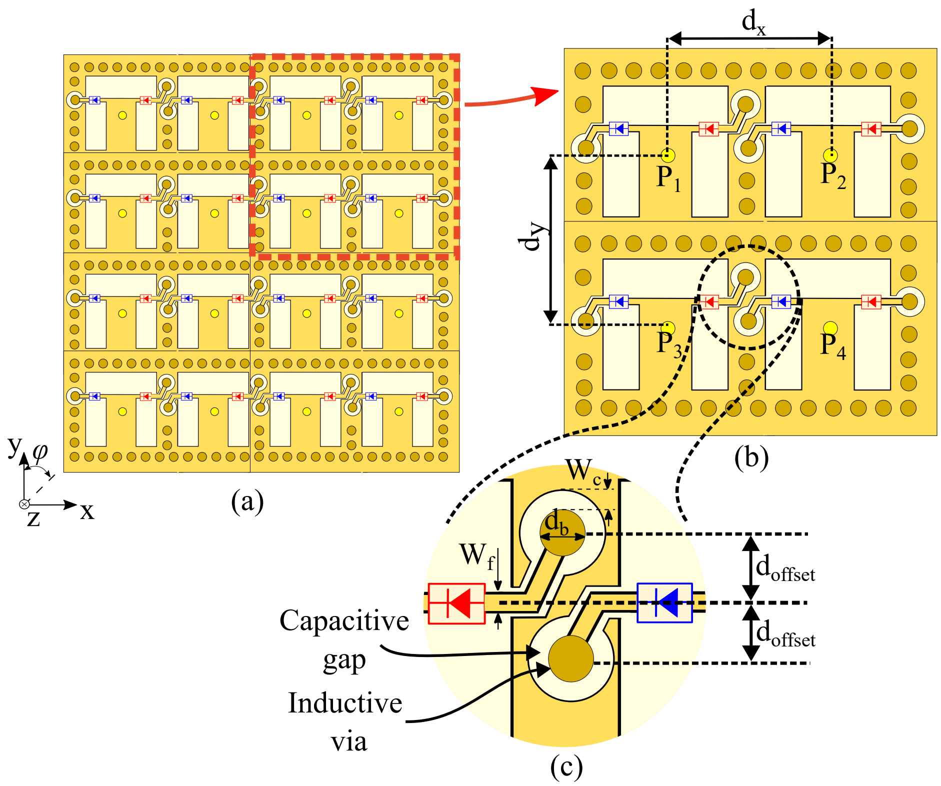

Figure 7: (a) a 4x4 polarization-reconfigurable antenna array design. (b) 2 × 2 sub-antenna array introducing a (c) DC biasing offset. Parameter values: $d_x = d_y = 22.5$ mm, $w_c = 0.15$ mm, $w_f = 0.2$ mm, $d_{offset} = 2$ mm and $d_b = 1.2$ mm.

The reconfigurable antenna is transformed into a planar polarization-reconfigurable array, particularly suited for compact FR3 wireless communication systems where polarization agility is needed. The small footprint and self-shielding characteristics owing to the guard wall of the proposed antenna element enable the implementation of a polarization-reconfigurable antenna array, as demonstrated in Fig. 7. To minimize inter-antenna-element spacing, the integrated bias-tee was slightly modified by applying an offset (d_{offset}) in the biasing lines connected to the diodes, as can be seen in in Fig. 7(c). The modification of the integrated bias-tee does not impact the AE performance. To later allow independent polarization control of the elements, the inter-element distance was fixed to 22.5 mm ($0.6\lambda_0$). This offset thus ensures maximal compactness by placing two elements as close as possible and allows for x- and y-spacing to remain equidistant ($d_x = d_y$). The vias also operate as guard walls between the elements, while allowing independent polarization control in the array. However, embedding an antenna element into an array configuration typically affects its performance, due to mutual coupling [39]. Hence, a modular antenna element that can be integrated into arrays without requiring extra optimization offers a clear advantage. The guard wall implemented during the single-element design phase provides this modularity by isolating the QM-AFSIW cavities from any neighboring elements. Therefore, our single-element antenna is analyzed while it is embedded into a 2×2, 3×3 and 4×4 antenna array without additional optimization.

Table 1 shows a comparison of the relevant simulated figures-of-merit for the antenna element in stand-alone conditions and when embedded in either a 2×2, 3×3 or 4×4 antenna array. Note that the impedance bandwidth of the antenna element remains approximately the same. The fractional bandwidth (FBW) of all the array elements lies between 8.31% and 9.16%, and every element remains matched in at least the 7.75 GHz - 8.25 GHz range. Hence, the proposed antenna element covers the targeted frequency band when embedded in either array. The mutual coupling between any two elements in the 2×2 array remains below -15.06 dB. An analysis of the element spacing with respect to mutual coupling has been performed. The two possible array configurations are shown in Fig. 8(a) and (b), while Fig. 8(c) illustrates the decreasing mutual coupling, reaching values as low as -25dB at an inter-element spacing of $1\lambda_0$. When placed inside the array, the boresight realized gain increases slightly, owing to the enlarged ground plane surrounding the elements, which provides improved directivity. The cross-polarization discrimination for the AE at boresight equals 15.4 dB, while, when embedded inside the array, the edge elements, cross-polarization discrimination deteriorates by 5 dB. If the desired application necessitates higher discrimination, the edge elements can be swapped for dummy elements to eliminate this deterioration [40]. The inner elements exhibit a maximum of 3 dB loss in cross-polarization discrimination. No inner elements exist for the 2×2 array. Radiation efficiency remains at 90% for each element when deployed in the array. Owing to its inherent self-shielding and based on the simulation results, the proposed antenna element retains its performance when embedded in array configurations.

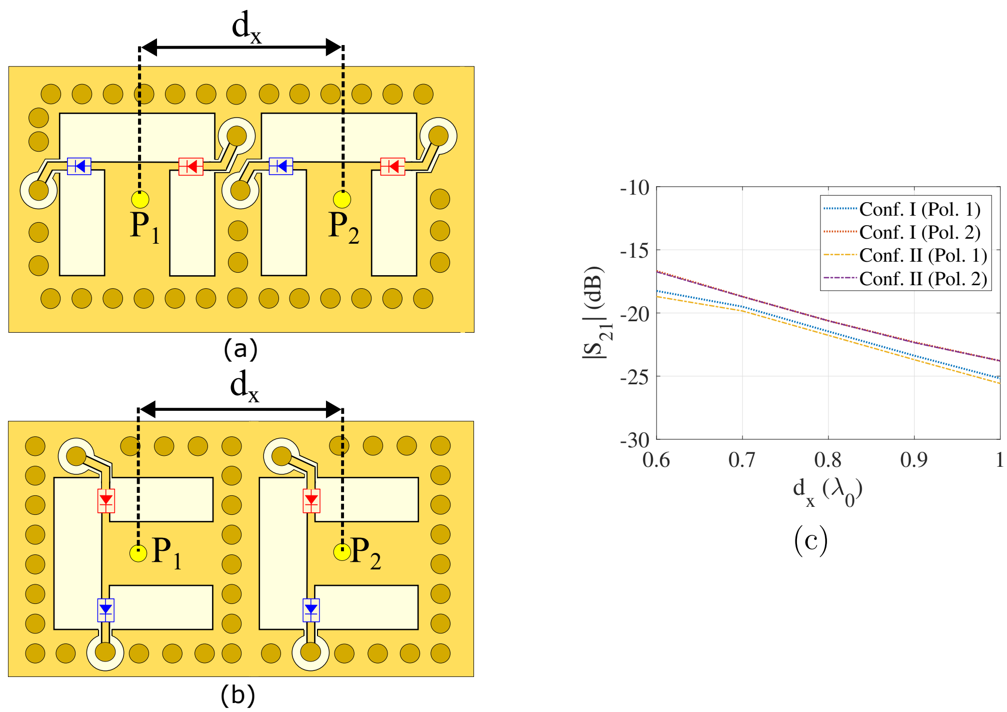

Figure 8: Analysis of impact of element spacing on mutual coupling $|S_{21}|$ between two adjacent polarization-reconfigurable AFSIW antenna elements with ports P_1 and P_2: (a) Configuration I (Conf. I) and (b) Configuration II (Conf. II). (c) Simulated mutual coupling $|S_{21}|$ at 8 GHz as a function of element spacing d_x normalized with respect to λ_0 for Pol. 1 (+45° linear polarization) and Pol. 2 (-45° linear polarization) states.

Fig. 9 shows simulated 2D-steering with uniform phase excitation for the 4×4 antenna array, with grating-lobe-free steering up to 40° in the elevation axis for two azimuth angles: (a) $\phi = 0°$, and (b) $\phi = 90°$. The polarization configuration was chosen to match to the radiation direction. All simulations were performed in Simulia CST microwave studio [41]. Broadside steering displays a gain of 16.6 dBi with a cross-polarization discrimination of 10dB.

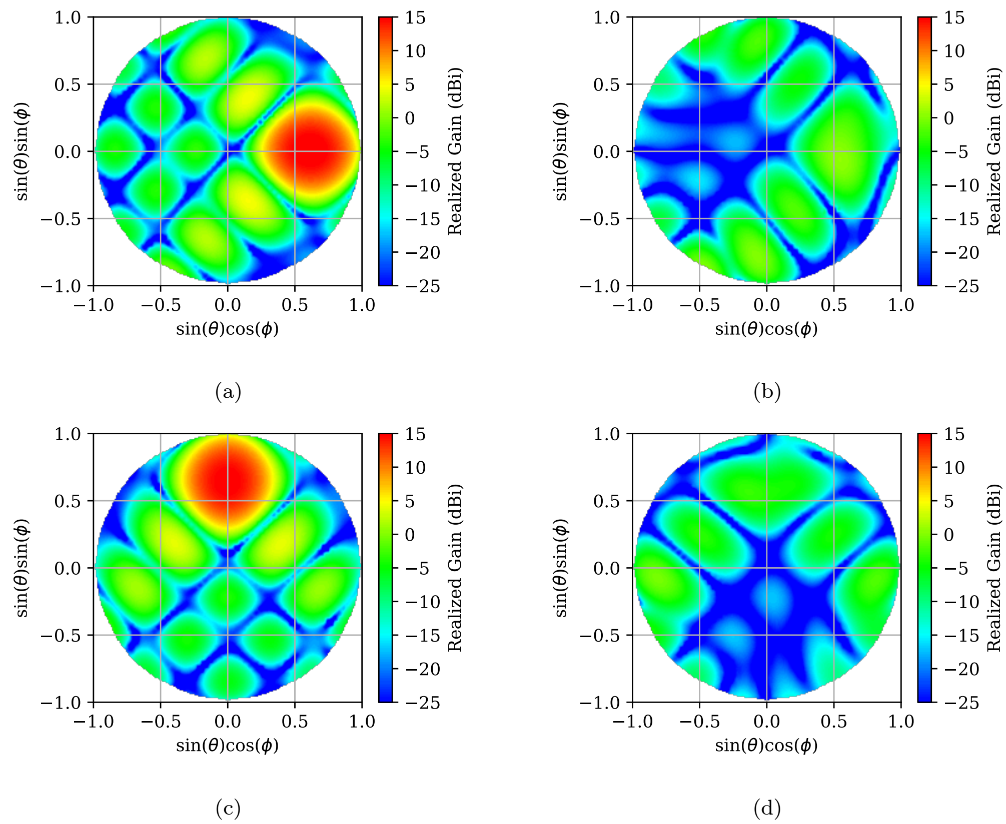

(a) (b) (c) (d)

Figure 9: Simulated Co/Cross-polarization 2D beam steering patterns of the 4×4 array at an elevation angle of $\theta = 40°$ for two azimuth angles. For $\phi = 0°$ at $+45$ degree polarization configuration: (a) Co-polarization, and (b) Cross-polarization; for $\phi = 90°$ in -45 degree polarization configuration: (c) Co-polarization, and (d) Cross-polarization.

Table 1: Performance comparison of a stand-alone antenna element and an antenna element embedded in a 2×2, 3×3, and 4×4 array. The table represents worst-case values over all elements.
AE: Antenna element; EE: Embedded element η_{rad}: Radiation efficiency

Figure-of-merit	**Single element**	**Array**		
		2 × 2	**3 × 3**	**4 × 4**
AE FBW (%)	8.22	9.16	8.38	8.31
Mut. coup. (dB)	-	>15.06	>15.59	>15.37
AE gain @ boresight (30°) (8 GHz) (dBi)	5.2	5.3	5.4	5.6
AE Co/X-pol disc. Edge EE @ boresight (30°) (8 GHz) (dB)	15.4	10.7	10.4	10.5
AE Co/X-pol disc. Inner EE @ boresight (30°) (8 GHz) (dB)	15.4	NA	14.5	12.5
AE $\eta_{\mathbf{rad}}$ (8 GHz) (%)	91	91	90	90

3. Experimental Validation

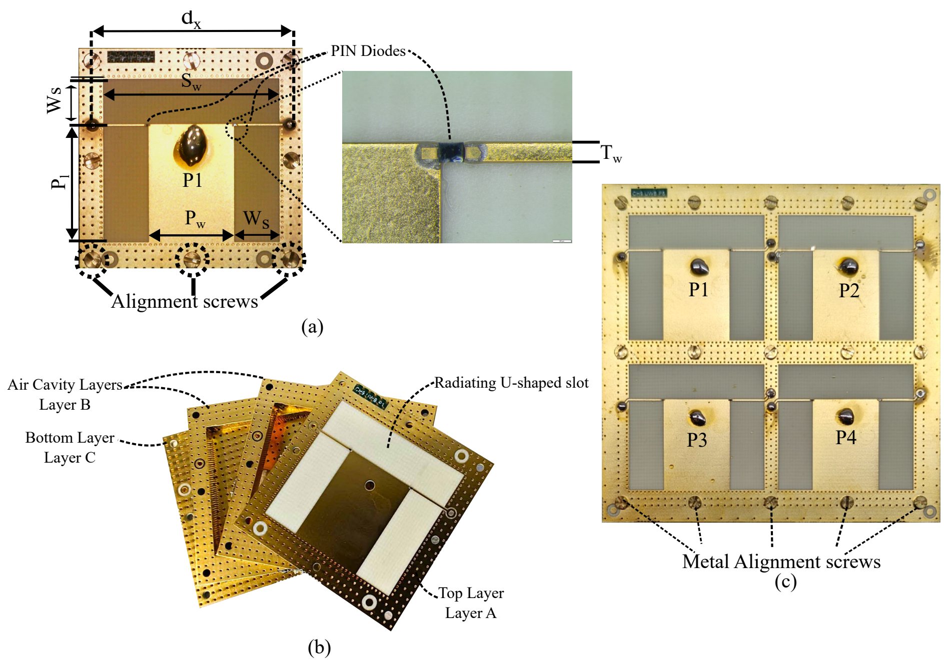

Figure 10: (a) Prototype of the stand-alone antenna element with zoom-in of the PIN diode placement. (b) PCB layers A, B and C, which together form the air-filled cavity. (c) Shows the fabricated 2×2 antenna array, where each element has the same dimensions as the single element. Parameter values: $d_x = 22.5$ mm, $W_s = 5.3$ mm, $S_w = 20.4$ mm, $P_l = 13.4$ mm, $P_w = 9.9$ mm, and $T_w = 0.2$ mm.

Antenna prototypes [see Fig. 10] are fabricated using a standard cost-effective printed circuit board (PCB) manufacturing process [42]. The antenna slot plane (layer A) and backplane (layer C) are implemented on a 0.254-mm-thick two-layer Rogers 4350B laminate [43], while the air cavity layers (layer B) are implemented through edge plating within a low-cost 3.24-mm-thick FR-4 dielectric laminate [44]. Notably, in this design, the bottom layer could alternatively be realized in FR-4 without affecting performance, as the substrate is shielded from antenna fields by the cavity ground plane implemented on its top layer. The bottom layer could also be replaced by a multilayer PCB, enabling the integration of a beam steering circuit with the necessary power planes and digital signaling [45]. All PIN diodes are soldered onto layer A (Fig. 10). In the final step, the three layers are assembled using metal alignment screws inserted through designated M1-size holes

(Fig. 10). These screws also enhance grounding conductivity between the top and bottom layers. The cavity is fully sealed, preventing humidity from penetrating and affecting antenna performance. When additional electronics are integrated on the backside of the antenna, the entire assembly should be placed within an enclosure to provide further protection against moisture.

To demonstrate scalability in both the x- and y-dimensions, a 2×2 array was fabricated using the same manufacturing technique as shown in Fig. 10 (c). The fabricated antenna element dimensions are represented in Fig. 10 (a).

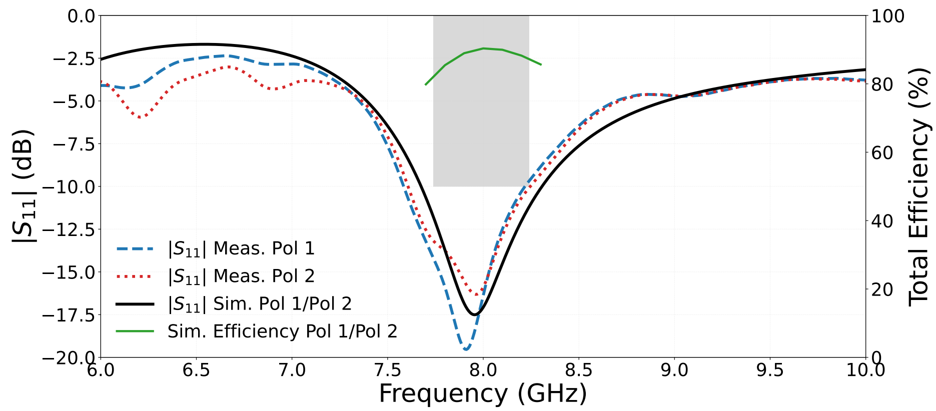

Figure 11: Reflection coefficient $|S_{11}|$ and total efficiency of stand-alone antenna element in both operating states, with the gray area indicating the targeted frequency band.

The S-parameters are measured using a Keysight N5242A PNA-X network analyzer, while the radiation performance is validated in an anechoic chamber with an NSI-MI spherical near-field antenna measurement system.

During measurements, the antenna was first evaluated under different bias currents, and it was observed that its performance remained unchanged once the current exceeded 3 mA. Given the forward voltage of 1.35 V for the MACOM PIN diodes, this corresponds to a very low power consumption of approximately 4 mW to achieve polarization reconfigurability. Since reverse biasing draws negligible current, the overall consumption remains at a minimal 4 mW. Furthermore, the MACOM PIN diodes support fast switching speeds of 5 ns, ensuring rapid reconfiguration.

Fig. 11 depicts the simulated and measured input reflection coefficients for both LP states of the single element, showing good agreement. In both states, the antenna maintains a 50 Ω match from 7.61 GHz to 8.20 GHz, achieving a -10 dB impedance bandwidth of 0.59 GHz (7.46%). A slight downward frequency shift is observed due to over-milling of the cavity; however, the entire [7.75–8.25] GHz band is still covered up to -9.5 dB. The simulated total efficiency in the frequency band is shown on the right side of Fig. 11 with a maximum of 91%.

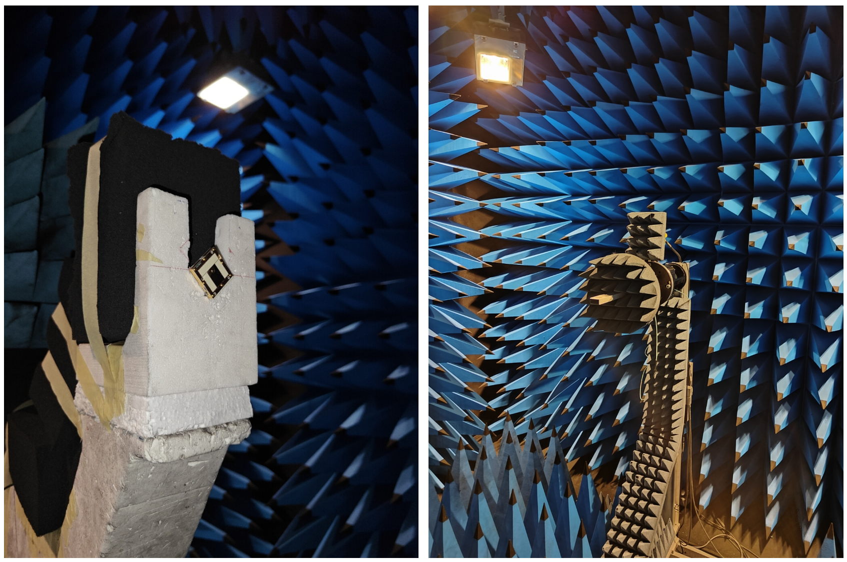

(a) (b)

Figure 12: (a) AUT mounting in anechoic chamber (b) probe mounting in anechoic chamber.

The radiation patterns of the single element are simulated and measured at the start, center and stop frequencies in the operating band, for both LP states. Fig. 12 (a) shows the mounting of our AUT in the anechoic chamber, together with the probe Fig. 12 (b) used to measure the co- and cross-polarization gain. The probe was calibrated using a standard gain horn antenna to accurately extract the realized gain of the antenna. Fig. 13 shows the measured and simulated radiation patterns at 8 GHz, the center frequency of the operating band. The figure demonstrates strong agreement between simulation and measurement, with a maximum gain of 5.18 dBi at 28° from broadside. Similar results were obtained at the start and end frequencies of the band. Each polarization state maintains a 3-dB beamwidth exceeding 78°.

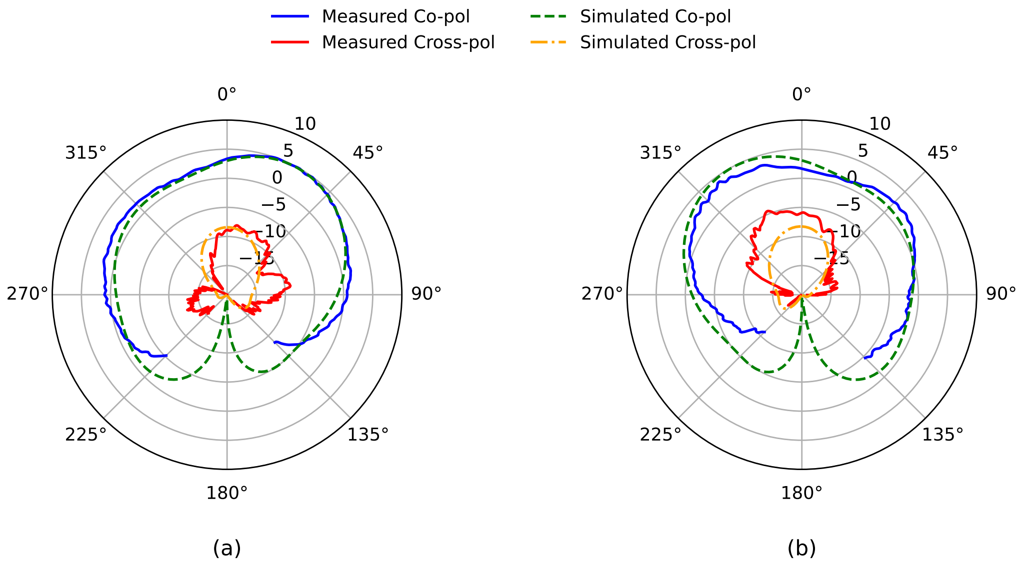

Figure 13: Measured and simulated realized gain (dBi) at 8 GHz of the stand-alone antenna element: (a) polarization 1 along the ϕ = -45°-plane and (b) polarization 2 along the $\phi = +45°$-plane.

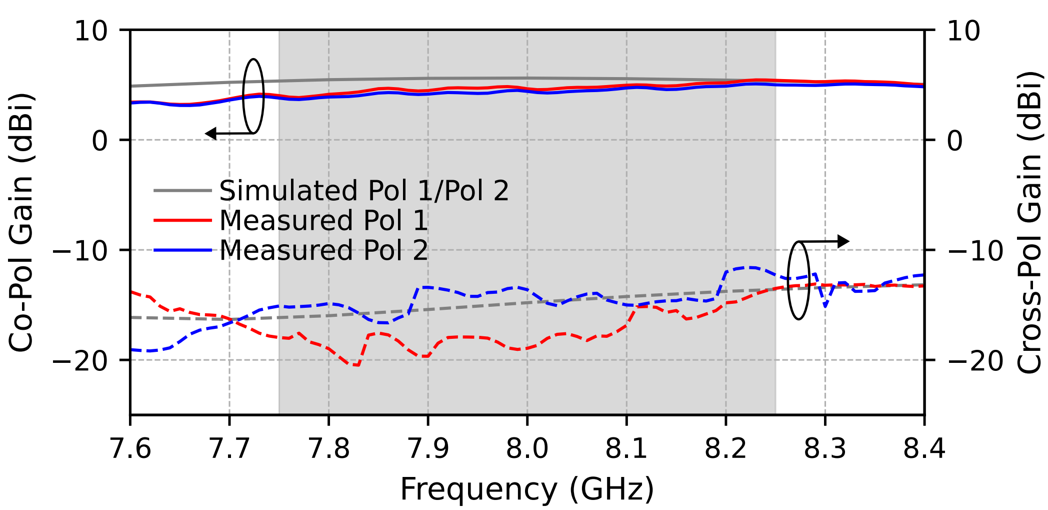

Figure 14: Boresight co-polarization and cross-polarization gain of the single antenna element as a function of frequency, demonstrating cross-polarization discrimination greater than 16.5 dB and a stable boresight gain of 4.51 ± 0.76 dBi over the entire band. A discrepancy smaller than 3 dB between simulation and measurement is observed, which is mainly due to fabrication tolerances and measurement setup conditions.

As represented in Fig. 14, the antenna ensures a boresight cross-polarization discrimination greater than 16.5 dB and the stand-alone antenna achieves a stable average boresight gain of 4.51 $\pm$ 0.76 dBi over the complete frequency band. Finally, the measured total antenna efficiency equals 91% for both the -45° LP and +45° LP states. Minor discrepancies between simulated and measured results in Fig. 8 mainly originate from fabrication tolerances, the soldering of the PIN diodes, and assembly misalignment, which introduce slight differences in the effective cavity dimensions. Nevertheless, the overall performance trends and design goals remain consistent.

For the 2×2 array Fig. 15 (a) shows the $|S_{ii}|$ for all four elements in both polarization states. The measured impedance bandwidth shows good agreement with simulation results, exhibiting a -10 dB bandwidth ranging from 7.75 to 8.25 GHz in most cases. In three edge cases, a slightly relaxed criterion of -9.5 dB is met within the upper 80 MHz portion of the band. Fig. 15 (b) represents the mutual coupling between the elements for both polarization states, remaining below -15 dB, demonstrating good isolation between all elements. The high isolation contributes to maintaining embedded element patterns that closely resemble those of the stand-alone antenna element, with only minor deviations. These results confirm that the integrated guard wall structure effectively suppress unwanted interactions between adjacent elements. The limited coupling not only minimizes distortion of the embedded element radiation patterns but also ensures stable array performance when scaling to larger configurations. Such isolation is particularly beneficial for polarization-reconfigurable arrays, as it maintains high polarization purity in both switching states.

Fig. 16 shows the far-field patterns for the antenna array elements in both polarization states at 8 GHz Importantly, the patterns shown minor differences across both the upper and lower portions of the operational band, indicating that the antenna's directional characteristics are stable throughout the frequency range. The embedded element realized gain in the array is measured to be between 4.04 and 5.35 dBi. Combining the far-field patterns of the 2×2 array shows a realized broadside gain of 9.5 dBi with a polarization discrimination of over 11 dB. The embedded element patterns demonstrate consistent performance within the array, showing low variation and minimal mutual coupling, owing to the 15 dB isolation between elements. This confirms their suitability as reliable building blocks for larger antenna arrays, supporting effective beamforming.

Table 2 compares the proposed polarization-reconfigurable AFSIW an-

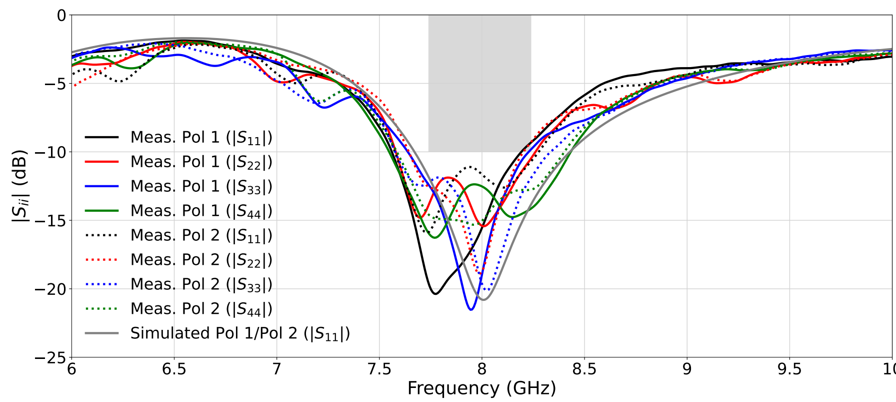

(a)

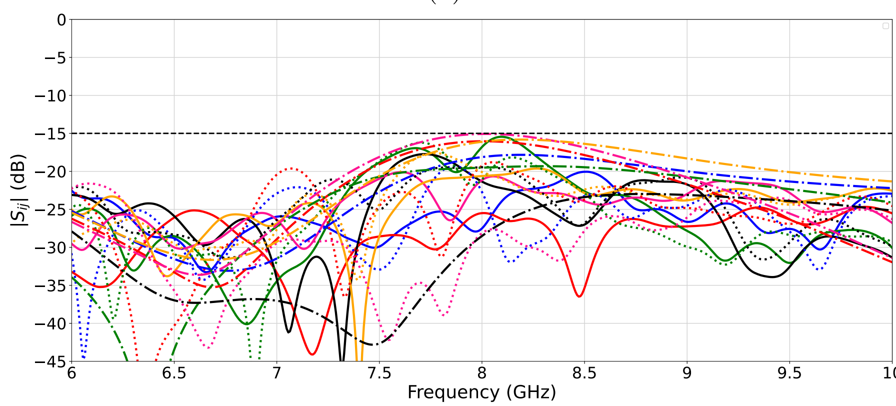

(b)

Figure 15: S-parameter performance of the 2×2 antenna array for both operating states: (a) $|S_{ii}|$ of an antenna element i, exhibiting a -10 dB reflection coefficient bandwidth ranging from 7.75 to 8.25 GHz except elaxed criterion of -9.5 dB in three edge cases. The gray area indicates the targeted frequency band. (b) Simulated and measured $|S_{ij}|$ between antenna elements i and j, remaining below -15 dB, demonstrating good isolation between all elements.

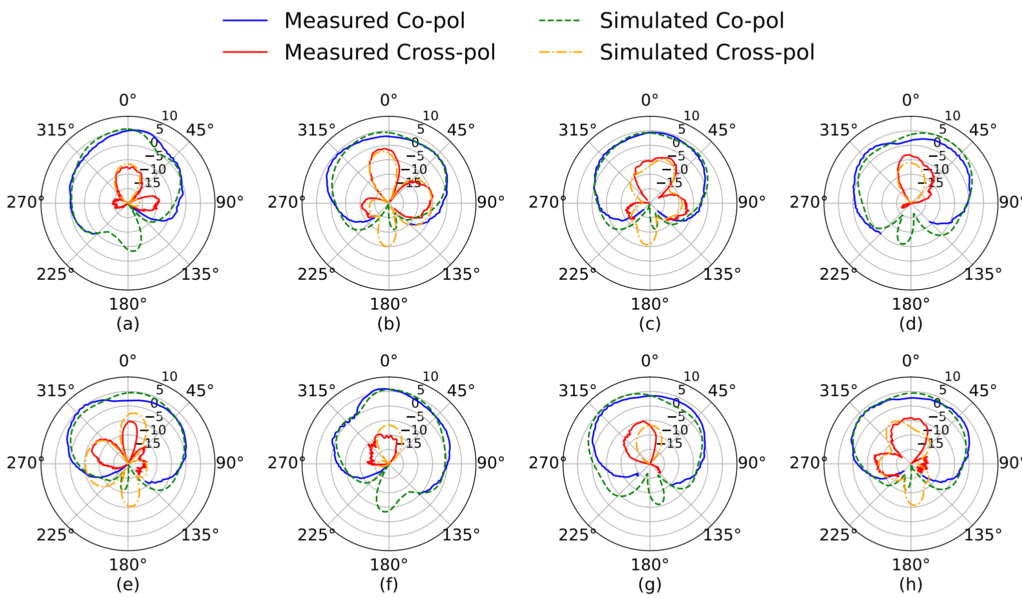

Figure 16: Measured and simulated realized gain (dBi) of the 2×2 array at 8 GHz Antenna 1: (a) Polarization 1 for the ϕ = -45°-plane and (e) Polarization 2 for the $\phi = +45°$-plane. Antenna 2: (b) Polarization 1 for the ϕ = -45°-plane and (f) Polarization 2 for the $\phi = +45°$-plane. Antenna 3: (c) Polarization 1 for the ϕ = -45°-plane and (g) Polarization 2 for the $\phi = +45°$-plane. Antenna 4: (d) Polarization 1 for the ϕ = -45°-plane and (h) Polarization 2 for the $\phi = +45°$-plane.

tenna in terms of performance and footprint with state-of-the-art polarization-reconfigurable (AF)SIW antennas described in literature. The antennas listed in this table operate at different frequency bands because each design was optimized for its specific application (e.g., WiFi, MIMO). Our proposed antenna targets the FR3 band for emerging 6G applications. It is demonstrated that our topology offers a compact footprint with high radiation efficiency and is the first to do so in this frequency band. While some of the referenced designs achieve higher antenna gain than our design's single element, they do so by relying on larger apertures, hindering beam steering applications. Moreover, our design uses just one diode per polarization state per element, which greatly reduces component cost. Finally, our approach is the only design that operates without requiring additional discrete biasing components. As a result, it can achieve polarization switching at the intrinsic 5 ns speed of the PIN diodes, whereas other reported designs do not specify their switching speed. This balance of performance metrics makes our design a strong candidate for future polarization-reconfigurable array systems.

Table 2: State-of-the-art polarization reconfigurable (AF)SIW antennas and arrays.

Ref.	**f_0 (GHz)**	**Footprint (λ_0^2)**	**FBW (%)**	**η_{tot} (%)**	**Gain (dBi)**	**# Pol. states**	**Method**	**Beam Steering**	**# Bias. comp.**
[46] AE	3.80	1.27×1.27	9.3	>93	7.6	Multi	6 PIN	Pol. Depend.	26
[47] AA	2.45	0.76×0.76	0.8	NA	4.3	2	2 PIN	No	6
[48] AE	2.45	0.36×0.36	1.2	NA	4.8	3	2 PIN	No	3
[36] AE	5.65	1.10×1.10	16.3	>95	7.3	2	8 PIN	No	Disc. BT
[31] AE	5.65	1.10×1.10	29	>70	5.2	4	16 PIN	No	Disc. BT
[19] AE	5.00	1.10×1.10	25.9	59	6.7	3	NA	No	3 RF Sw.
[29] AE	2.40	0.90×0.80	1.2	39.9	4.7	4	48 PIN	No	32
[26] AE	1.68	0.67×0.67	0.11	NA	10	2	LM	No	NA
[33] AA	8.36	0.70×0.70	3.1	54.5	6	3	8 PIN	No	16
[18] AA	5.80	2.90×2.30	3.08	54.5	8.56	3	18 PIN	No	12
[34] AE	2.4	1.44×1.44	10.87	NA	4.7	3	12 PIN	No	12
T.W. AE	**8.00**	**0.6×0.6**	**7.46**	**91**	**5.4**	**2**	**2 PIN**	NA	**0**
T.W. 2×2	**8.00**	**1.20×1.20**	**7.46**	**78**	**9.5**	**2**	**8 PIN**	Yes	**0**

AE: Antenna element; AA: antenna array; f_0: Center frequency; FBW: Fractional bandwidth; η_{tot}: Total efficiency; LM: Liquid metal; # Bias. Comp.: Number of biasing components.; Disc. BT: Discrete Bias-Tee; RF Sw.: RF Switch; T.W.: This work.

4. Conclusion

A compact, highly efficient polarization-reconfigurable QM-AFSIW AE was proposed and validated for operation in the [7.75–8.25] GHz band. The design leverages an edge-plated AFSIW cavity fabricated using cost-effective dual-layer PCB technology, achieving a high total efficiency exceeding 90% across a -10 dB impedance bandwidth of 7.46%. The integration of an innovative biasing network eliminates the need for discrete components, simplifying implementation, while maintaining stable performance. By switching between two orthogonal polarizations, the antenna effectively mitigates polarization mismatch losses, preventing complete signal degradation. This characteristic enhances link reliability, making it particularly well-suited for future space-constrained FR3 wireless communication systems. The proposed design is inherently scalable, allowing for seamless expansion to larger antenna arrays, as proven by the fabricated 2×2 antenna array. The AE's compact footprint ($0.6\lambda_0 \times 0.6\lambda_0$) and high efficiency make it an excellent candidate for future beamforming applications, as was demonstrated by the simulated performance of a 4×4 array. Experimental validation of a 2×2 array confirmed realized broadside gain of 9.5 dBi, good polarization purity, and at least -15 dB isolation between adjacent elements. Overall, the proposed QM-AFSIW AE offers a highly efficient, compact, and scalable solution for polarization-reconfigurable FR3 antenna arrays.

References

[1] K. Wu, H. Zhang, Y. Chen, Q. Luo, K. Xu, All-silicon microdisplay using efficient hot-carrier electroluminescence in standard 0.18µm CMOS technology, IEEE Electron Device Letters 42 (4) (2021) 541–544. doi:10.1109/LED.2021.3059781.

[2] V. Suryapaga, V. V. Khairnar, Review on multifunctional pattern and polarization reconfigurable antennas, IEEE Access 12 (2024) 90218–90251. doi:10.1109/LAWP.2024.3447230.

[3] C. Wu, C.-F. Lai, A survey on improving the wireless communication with adaptive antenna selection by intelligent method, Computer Communications 181 (2022) 374–403. doi:10.1016/j.comcom.2021.10.034.

[4] E. Björnson, F. Kara, N. Kolomvakis, A. Kosasih, P. Ramezani, M. B. Salman, Enabling 6G performance in the upper mid-band by transitioning from massive to gigantic MIMO, IEEE Open Journal of the Communications Society 6 (2025) 5450–5463. doi:10.1109/OJCOMS.2025.3576931.

[5] F. Parment, A. Ghiotto, T.-P. Vuong, J.-M. Duchamp, K. Wu, Air-filled substrate integrated waveguide for low-loss and high power-handling millimeter-wave substrate integrated circuits, IEEE Transactions on

Microwave Theory and Techniques 63 (4) (2015) 1228–1238. doi:10.1109/TMTT.2015.2408593.

[6] L. Li, J.-B. Yan, A low-cost and efficient microstrip-fed air-substrate-integrated waveguide slot array, Electronics 10 (3) (2021). doi:10.3390/electronics10030338.

[7] L. Van Messem, S. Sinha, I. Ocket, H. Trischler, E. Schlaffer, D. Schlick, H. Rogier, S. Lemey, Air-filled SIW technology for mass-manufacturable and energy-efficient terahertz systems, Scientific Reports 13 (1) (2023) 16714. doi:10.1038/s41598-023-43887-0.

[8] M. Bozzi, A. Georgiadis, K. Wu, Review of substrate-integrated waveguide circuits and antennas, IET Microwaves, Antennas & Propagation 5 (2011) 909–920. doi:10.1049/iet-map.2010.0463.

[9] M. Bozzi, A. Georgiadis, K. Wu, Review of substrate-integrated waveguide circuits and antennas, IET Microwaves, Antennas & Propagation 5 (8) (2011) 909–920. doi:10.1049/iet-map.2010.0463.

[10] Z. Xu, J. Liu, S. Huang, Y. Li, Gain-enhanced SIW cavity-backed slot antenna by using TE410 mode resonance, AEU - International Journal of Electronics and Communications 98 (2019) 68–73. doi:10.1016/j.aeue.2018.10.039.

[11] B. Wang, Z. Zhao, K. Sun, T. Tao, X. Yang, D. Yang, Low-profile high-aperture-efficiency air-filled substrate integrated cavity antenna array, IEEE Antennas and Wireless Propagation Letters 21 (7) (2022) 1442–1446. doi:10.1109/LAWP.2022.3171182.

[12] T. Martin, A. Ghiotto, T.-P. Vuong, F. Lotz, Self-temperature-compensated air-filled substrate-integrated waveguide cavities and filters, IEEE Transactions on Microwave Theory and Techniques 66 (8) (2018) 3611–3621. doi:10.1109/TMTT.2018.2851243.

[13] S. A. Ali, M. Wajid, A. Kumar, M. Shah Alam, Design challenges and possible solutions for 5G SIW MIMO and phased array antennas: A review, IEEE Access 10 (2022) 88567–88594. doi:10.1109/ACCESS.2022.3197226.

[14] I. Lima de Paula, S. Lemey, D. Bosman, Q. Van den Brande, O. Caytan, J. Lambrecht, M. Cauwe, G. Torfs, H. Rogier, Cost-effective high-performance air-filled SIW antenna array for the global 5G 26 GHz and 28 GHz bands, IEEE Antennas and Wireless Propagation Letters 20 (2) (2021) 194–198. doi:10.1109/LAWP.2020.3044114.

[15] M. K.N., Y. K. Choukiker, Dual-mode aperture-coupled patch resonator based dual-band higher-order frequency selective surfaces, AEU - International Journal of Electronics and Communications 177 (2024) 155171. doi:10.1016/j.aeue.2024.155171.

[16] T. Wu, Z. Zhang, W.-J. Wang, M.-J. Wang, Coupling suppression study of miniaturized BDS/GPS multifunctional transceiver antenna based on quarter-mode substrate integrated waveguide, AEU - International Journal of Electronics and Communications 158 (2023) 154461. doi:10.1016/j.aeue.2022.154461.

[17] G.-J. Gordebeke, S. Lemey, O. Caytan, M. Boes, J. Jocqué, S. Van de Velde, C. Marshall, E. De Poorter, H. Rogier, Time-domain-optimized antenna array for high-precision IR-UWB localization in harsh urban shipping environments, IEEE Sensors Journal 24 (5) (2024) 5561–5577. doi:10.1109/JSEN.2023.3310992.

[18] Z.-C. Hao, K.-K. Fan, H. Wang, A planar polarization-reconfigurable antenna, IEEE Transactions on Antennas and Propagation 65 (4) (2017) 1624–1632. doi:10.1109/TAP.2017.2670440.

[19] W.-J. Sun, W.-W. Yang, L. Guo, W. Qin, J.-X. Chen, A circularly polarized dielectric resonator antenna and its reconfigurable design, IEEE Antennas and Wireless Propagation Letters 19 (7) (2020) 1088–1092. doi:10.1109/LAWP.2020.2989156.

[20] A. Singh, R. Dubey, Ajitesh, S. Kumar Srivastava, M. Kumar Meshram, Circular polarization-agile and beam switching enabled reconfigurable cavity-backed antenna, AEU - International Journal of Electronics and Communications 165 (2023) 154664. doi:10.1016/j.aeue.2023.154664.

[21] M. P. Singh, T. Tomura, J. Hirokawa, S. Ghosh, A compact wide-band millimeter-wave polarization-reconfigurable antenna array, IEEE

Antennas and Wireless Propagation Letters 24 (3) (2025) 691–695. doi:10.1109/LAWP.2024.3512792.

[22] W. Tang, X. Gao, C. Ding, C. Zhu, R. Li, B. Tian, X. Bu, J. An, A quad-polarization reconfigurable conformal array of wide coverage range and high gain for unmanned aerial vehicle communications, IEEE Transactions on Antennas and Propagation 72 (4) (2024) 3795–3800. doi:10.1109/TAP.2024.3371680.

[23] E. Al Abbas, N. Nguyen-Trong, A. T. Mobashsher, A. M. Abbosh, Polarization-reconfigurable antenna array for millimeter-wave 5G, IEEE Access 7 (2019) 131214–131220. doi:10.1109/ACCESS.2019.2939815.

[24] J.-S. Row, Y.-H. Wei, Wideband reconfigurable crossed-dipole antenna with quad-polarization diversity, IEEE Transactions on Antennas and Propagation 66 (4) (2018) 2090–2094. doi:10.1109/TAP.2018.2800785.

[25] Y. J. Guo, P.-Y. Qin, S.-L. Chen, W. Lin, R. W. Ziolkowski, Advances in reconfigurable antenna systems facilitated by innovative technologies, IEEE Access 6 (2018) 5780–5794. doi:10.1109/ACCESS.2017.2789199.

[26] M. Wang, X. Fu, A. Chen, Differential-fed circularly polarized reconfigurable SIW antenna by using liquid metal, IEEE Antennas and Wireless Propagation Letters 23 (11) (2024) 3714–3718. doi:10.1109/LAWP.2024.3447230.

[27] Y. Liu, Q. Wang, Y. Jia, P. Zhu, A frequency- and polarization-reconfigurable slot antenna using liquid metal, IEEE Transactions on Antennas and Propagation 68 (11) (2020) 7630–7635. doi:10.1109/TAP.2020.2993110.

[28] W. Zhu, X. Liu, Y. Fan, Z. Zhang, X. Ma, Transparent and flexible antenna with polarization reconfigurability using EGaIn for wearable applications, IEEE Transactions on Antennas and Propagation 72 (10) (2024) 7493–7503. doi:10.1109/TAP.2024.3439882.

[29] L. Ge, Y. Li, J. Wang, C.-Y.-D. Sim, A low-profile reconfigurable cavity-backed slot antenna with frequency, polarization, and radiation pattern agility, IEEE Transactions on Antennas and Propagation 65 (5) (2017) 2182–2189. doi:10.1109/TAP.2017.2681432.

[30] A. Bharathi, G. Ravi Shankar Reddy, A novel dual-sense polarization reconfigurable dual-band microstrip antenna, AEU - International Journal of Electronics and Communications 171 (2023) 154926. doi:10.1016/j.aeue.2023.154926.

[31] K. Y. Kapusuz, S. Lemey, H. Rogier, Multipolarization-reconfigurable air-filled substrate integrated waveguide cavity-backed slot antenna, IEEE Antennas and Wireless Propagation Letters 20 (4) (2021) 622–626. doi:10.1109/LAWP.2021.3059449.

[32] Z. Wu, L. Li, W. Wu, J. J. Liang, L. L. Huang, Ultrawideband polarization-reconfigurable antenna based on C-shaped radiators, IEEE Antennas and Wireless Propagation Letters 24 (1) (2025) 113–116. doi:10.1109/LAWP.2024.3485491.

[33] J. Hu, Z.-C. Hao, Z.-W. Miao, Design and implementation of a planar polarization-reconfigurable antenna, IEEE Antennas and Wireless Propagation Letters 16 (2017) 1557–1560. doi:10.1109/LAWP.2017.2650961.

[34] Y. Wu, H. Sun, A low-profile wideband omnidirectional antenna with reconfigurable tri-polarization diversity, AEU - International Journal of Electronics and Communications 176 (2024) 155149. doi:10.1016/j.aeue.2024.155149.

[35] Q. Ren, Y. Liu, P. Guo, S.-L. Chen, A wideband switchable l-probe patch antenna with reconfigurable twelve linear polarizations and dual circular polarizations, IEEE Antennas and Wireless Propagation Letters 23 (11) (2024) 3506–3510. doi:10.1109/LAWP.2024.3491313.

[36] K. Y. Kapusuz, S. Lemey, A. Petrocchi, P. Demeester, D. Schreurs, H. Rogier, Polarization reconfigurable air-filled substrate integrated waveguide cavity-backed slot antenna, IEEE Access 7 (2019) 102628–102643. doi:10.1109/ACCESS.2019.2926809.

[37] Q. Van den Brande, S. Lemey, J. Vanfleteren, H. Rogier, Highly Efficient Impulse-Radio Ultra-Wideband Cavity-Backed Slot Antenna in Stacked Air-Filled Substrate Integrated Waveguide Technology, IEEE Transactions on Antennas and Propagation 66 (5) (2018) 2199–2209. doi:10.1109/TAP.2018.2809626.

[38] MA4AGBLP912.
URL https://www.macom.com/products/product-detail/MA4AGBLP912

[39] T. Latha, G. Ram, G. A. Kumar, M. Chakravarthy, Review on ultra-wideband phased array antennas, IEEE Access 9 (2021) 129742–129755. doi:10.1109/ACCESS.2021.3114344.

[40] M. Kohtani, S. Cha, P. Schmalenberg, J. Lee, L. Li, T. Takahata, S. Yamaura, T. Matsuoka, G. M. Rebeiz, Thinned array with steerable nulls to cancel grating lobe for automotive radar applications, in: 2022 52nd European Microwave Conference (EuMC), 2022, pp. 385–388. doi:10.23919/EuMC54642.2022.9924319.

[41] CST Studio Suite (2023).
URL https://www.3ds.com/products/simulia/cst-studio-suite

[42] Making a PCB - PCB Manufacture Step-by-Step.
URL https://34.252.181.249/making-a-pcb-pcb-manufacture-step-by-step/

[43] RO4350B™ Laminates.
URL https://rogerscorp.com/advanced-electronics-solutions/ro4000-series-laminates/ro4350b-laminates

[44] IS400 Laminate and Prepreg.
URL https://www.isola-group.com/pcb-laminates-prepreg/is400-laminate-and-prepreg-isola-group/

[45] L. Van Messem, A. Moerman, O. Caytan, H. Rogier, S. Lemey, Compact self-shielding components for beamforming networks implemented in substrate integrated coaxial line technology, IEEE Transactions on Components, Packaging and Manufacturing Technology 15 (1) (2025) 15–21. doi:10.1109/TCPMT.2024.3436545.

[46] S. Danesh, M. Abedian, M. Khalily, P. Xiao, R. Tafazolli, A. A. Kishk, Polarisation reconfigurable anisotropic dielectric resonator antenna, Scientific Reports 15 (1) (2025) 11106. doi:10.1038/s41598-025-94491-3.

[47] T. Le-Tuan, T. D. Nguyen, N. V.-D. Tran, H. Tran, D. Nguyen-Tien, Circularly Polarized Reconfigurable MIMO Antenna for WLAN Applications, Sensors 25 (4) (2025) 1257. doi:10.3390/s25041257.

[48] T. Nguyen-Dinh, T. Dao-Duc, D. Nguyen-Quoc, H. Tran-Huy, N. Hussain, A method to design polarization reconfigurable antenna with simple switching mechanism and compact size characteristics, Scientific Reports 15 (1) (2025) 13387. doi:10.1038/s41598-025-97908-1.